Macromolecules

Article

pubs.acs.org/Macromolecules

Rational Design of Versatile Self-Assembly Morphology of Rod−Coil Block Copolymer

Shih-Hsiang Lin, Shang-Jung Wu, Chun-Chih Ho,* and Wei-Fang Su*

Department of Materials Science and Engineering, National Taiwan University, Taipei 106, Taiwan

Supporting Information

ABSTRACT: Controlling the nonlamellar and bicontinuous nanostructures through changing volume fraction is a well-developed technique for coil−coil block copolymer, but it is not always effective for rod−coil block copolymer due to strong rod−rod interaction. Versatile self-assembly morphology of rod−coil copolymer can be achieved by simultaneously adjusting the rod−rod interaction, rod−coil interaction, and conformational asymmetry. This approach has been investigated by using poly(3-alkylthiophene)-*b*-poly(methyl methacrylate) as a model. By altering the alkyl side chain of polythiophene from linear hexyl to longer dodecyl and to branch 2-ethylhexyl, both rod−coil and rod−rod interaction are decreased with increasing spatial occupation of alkyl side chain which have been quantitatively determined for this type of rod−coil copolymer. With tunable conformational asymmetry, competition between rod−rod and rod−coil interactions, and crystallization-driven force, the presence of versatile morphology, i.e., lamellar and hexagonal structures, cylinder-to-gyroid phase transition, and disordered phase, can be observed for long-sought composition at approximately $f_{rod} = 0.5$. The finding described here can provide new insights into the self-assembly behaviors of rod−coil block copolymer for scientists to manipulate and obtain the desired order morphology in high performance optoelectronic applications.

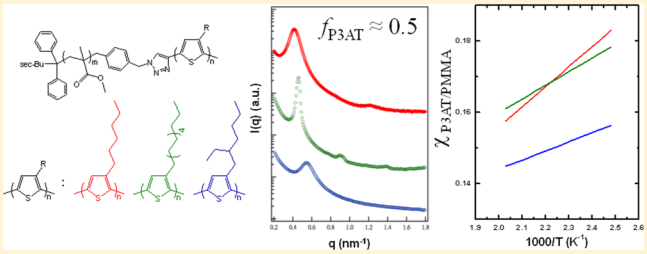

INTRODUCTION

The block copolymers can be self-assembled into a variety of ordered and periodic nanostructures which has drawn lots of attention for fundamental research.[1] They also become promising materials for advanced applications in lithography,[2] membranes,[3,4] optoelectronic devices,[5−7] and solar cells.[8−11] Not only classical structures, such as alternating lamellae, hexagonally packed cylinder, and body-centered cubic phase, but also complex structures, like perforated layer, gyroid, and diamond, can be observed through changing the volume fraction of one component (f) in conventional coil−coil block copolymer.[12] The phase diagram of PS-*b*-PI has been obtained by plotting χN vs f (where χ is the Flory−Huggins interaction parameter associated with repulsion between segments and N is the total number of volumetric repeat units). The lamellar structure was observed in large volume fraction window.[13] Most of theoretical work of phase behavior of block copolymer assumes an equal statistical segmental length of each block. However, another parameter of conformational asymmetry (ε) has been found to have a significant influence on the phase behavior of block copolymer experimentally.[14−17] This important parameter can be used to clarify the difference in the volume filling between two blocks, associated with unperturbed radius of gyration of each block. For a series of polyolefin diblock copolymers, the gyroidal structure is observed at $f_{PEE} = 0.57−0.60$ in polyethylene-*b*-polyethylethylene (PE-*b*-PEE) ($\varepsilon = 2.5$) while it is only found at $f_{PEE} = 0.60$ in poly(ethylene−propylene)-*b*-polyethylethylene (PEP-*b*-PEE) ($\varepsilon = 1.7$).[16] Furthermore, a highly asymmetric phase diagram of poly(1,2-octylene oxide)-*b*-poly(ethylene oxide) (POO-*b*-PEO) ($\varepsilon = 3.56$) reveals hexagonal and gyroidal structures near $f_{PEO} = 0.5$.[18]

If one of coil blocks is replaced by the rod segment composed of π-conjugated conducting backbone[19−21] or helical secondary structure,[22,23] the spatial occupation of chain conformation will be very different. Similar to ε affecting the phase behavior of conventional coil−coil block copolymer, the more significant mismatch in scaling dimension between the rod and coil has a profound influence on the self-assembled behavior of rod−coil block copolymer. By including two additional parameters, μ and G (where μ is the Maier−Saupé (rod−rod) interaction parameter and G is the competition between μ and χ), in the phase behavior studies of block copolymers, more complicated phases, e.g., zigzags, arrowheads, smectic A-like structures, gyroid, and smectic C, are observed.[24−28] Meanwhile, the elaborate self-assembly of rod−coil polymeric systems has been investigated based on the poly(diethylhexyloxy-*p*-phenylenevinylene) (DEH−PPV)-containing block copolymers with different segregation strengths by tuning rod−coil interactions but at constant rod−rod interaction.[21,29−32] The lamellar structures and liquid crystalline transitions are observed in a wide range of coil

Received: October 24, 2012
Revised: March 12, 2013
Published: March 22, 2013

   dx.doi.org/10.1021/ma302220b | *Macromolecules* 2013, 46, 2725−2732

fraction of copolymers (up to 0.8 coil fractions) because of the strong rod−rod interaction of DEH−PPV. The nonlamellar phases including hexagonal and spherical structures are found for high coil fraction of copolymers with increased segregation strength or less difference of packing geometry.[33] However, the comprehensive study of phase behaviors affected by conformational asymmetry and the competition between rod−rod and rod−coil interactions with tunable μ and χ parameters is still lacking. More importantly, at high coil fraction of rod−coil copolymer, the unique optoelectronic properties associated with the conjugating rod segment are diminishing due to the insulating characteristic of coil segment. There is an urgent need to provide a rational design of rod−coil copolymer with versatile morphology at approximately equal fraction of each segment for high performance optoelectronic applications.

In this article, we employed P3AT-*b*-PMMA as a model of rod−coil block copolymer via altering chemical structures of P3AT blocks to simultaneously adjust the rod−rod interaction of P3ATs, rod−coil interaction between P3AT and PMMA segments, and conformational asymmetry. We show, through the rational molecular design of rod−coil block copolymer, versatile self-assembly phase behaviors are achievable. Three kinds of P3ATs possessing different structures of alkyl side chain were designed and synthesized for this study, i.e., poly(3-hexylthiophene) (P3HT), poly(3-dodecylthiophene) (P3DDT), and poly(3-(2-ethylhexyl)thiophene) (P3EHT). In our previous work,[34] the temperature of order−disorder transition (T_{ODT}) for P3DDT-*b*-PMMA was not observed above 280 °C due to the strong interaction between P3DDT and PMMA segments. In order to investigate the order−disorder transition without thermal decomposition, we synthesized a series of P3AT-*b*-PMMA with low N values via click chemistry and PMMA coil volume fraction (f_{PMMA}) around 0.5. By using small-angle X-ray scattering (SAXS) profiles and transmission electron microscopy (TEM) images, we characterized and observed copolymers with various morphologies which were associated with the effects of the conformational asymmetry, competition between rod−rod and rod−coil interactions, and crystallization-driven force. It should be noted that since we introduced the alkyl side chain on the 3-position of thiophene, the chain rigidity of polythiophene could be reduced.

RESULTS AND DISCUSSION

A series of model rod−coil block copolymers with nearly compositional symmetry, P3AT-*b*-PMMA, were synthesized via Grignard metathesis polymerization (GRIM)[35] of P3AT and anionic polymerization of PMMA,[36] followed by click chemistry. Three kinds of P3ATs with different alkyl side chains used in this study are poly(3-hexylthiophene) (P3HT), poly(3-dodecylthiophene) (P3DDT), and poly(3-(2-ethylhexyl)thiophene) (P3EHT). Their chemical structures are shown in Scheme 1, and their molecular parameters and phase behaviors are summarized in Table 1. A denotation system $H_XM_Y(Z)$ is used to describe the compositions of P3HT-*b*-PMMA, where X and Y are the degree of polymerization (repeat unit) of P3HT and PMMA blocks, respectively, and Z is the volume fraction of PMMA (f_{PMMA}). DM and EM are the designations of P3DDT-*b*-PMMA and P3EHT-*b*-PMMA, respectively. Thus, $D_XM_Y(Z)$ and $E_XM_Y(Z)$ denotations describe the compositions of respective copolymers.

Figure 1a shows the synchrotron-SAXS profiles of a series of P3AT-*b*-PMMA at 30 °C. Each sample was thermally annealed

Scheme 1. Synthesis of P3AT-*b*-PMMA Rod−Coil Block Copolymers via Click Chemistry[a]

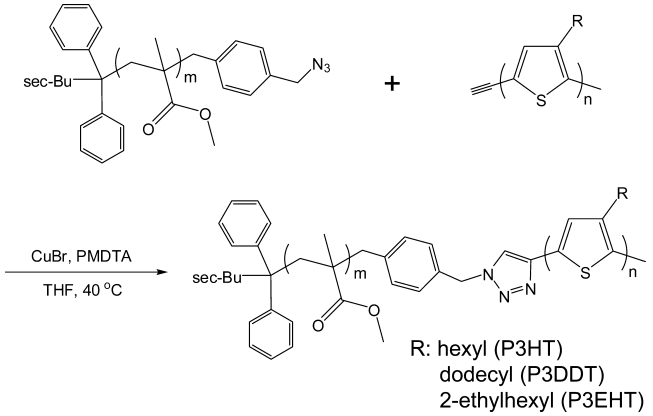

[a]Three kinds of P3ATs with different alkyl side chains used in this study are poly(3-hexylthiophene) (P3HT), poly(3-dodecylthiophene) (P3DDT), and poly(3-(2-ethylhexyl)thiophene) (P3EHT).

before each profile was collected. The SAXS profile of P3HT-*b*-PMMA with the composition of $H_{21}M_{35}(0.49)$ displays the scattering peaks associated with lamellar (LAM) structure without secondary peak, suggesting that the lamellar structure is nearly symmetrical. The lamellar morphology of $H_{21}M_{35}(0.49)$ is observed in the TEM image (Figure S1). While changing the side chain of rod segment from hexyl to dodecyl with more flexibility, the morphology of $D_{16}M_{47}(0.53)$ shows a unclear hexagonally packed cylinders (HEX) structure with weak peak at q value of $\sqrt{3}$ (as indicated by arrow). This depressed peak of $\sqrt{3}$ may be the result of the domain form factor. The TEM image of $D_{16}M_{47}(0.53)$ (Figure 2a) reveals different orientations of cylinders within different grains. When the side chain of rod segment is bulky such as 2-ethylhexyl, there is more spacing for curvature structure formation. The SAXS curve of $E_{19}M_{47}(0.52)$ shows significant multiple scattering peaks with position ratio of $1:\sqrt{3}:\sqrt{4}:\sqrt{7}$. The result clearly indicates that the $E_{19}M_{47}(0.52)$ exhibits a HEX morphology, where the minority of P3EHT cylinders are dispersed within the PMMA matrix. However, $E_{16}M_{35}(0.50)$ has a slightly lower molecular weight than $E_{19}M_{47}(0.52)$, its SAXS profile shows no highly ordered peaks, suggesting that this composition is located within the disordered regime (DIS) of the phase diagram.

The phase transition and the segregation strength of P3AT-*b*-PMMA were investigated by the temperature-dependent SAXS measurement to determine the thermodynamic stability of the phases and their transitions. Figure 1b−d displays the SAXS profiles of $E_{19}M_{47}(0.52)$, $D_{16}M_{47}(0.53)$, and $H_{21}M_{35}(0.49)$ at different temperatures upon heating. For $E_{19}M_{47}(0.52)$ at 150 °C (Figure 1b), it reveals the hexagonal morphology with sharp peaks at q values of 1, $\sqrt{3}$, and $\sqrt{4}$. As temperature increases to 170 °C, a new peak near the primary peak appears, and the SAXS profile shows clear scattering peaks with the position ratio of $\sqrt{3}:\sqrt{4}:\sqrt{7}:\sqrt{8}:\sqrt{10}:\sqrt{11}:\sqrt{12}$, indicating the formation of gyroidal phase. This gyroidal phase is further confirmed by the TEM experiment as shown in Figure 2c. The order−order transition (OOT) of P3EHT-*b*-PMMA, from cylinder to gyroid, is also observed in P3DDT-*b*-PMMA[34] and P3HT-*b*-P2VP[37,38] with high coil fraction. Upon further increasing the temperature, the intensity of all peaks of gyroid starts to decrease at 175 °C and then the peaks at high q values, disappearing at 180 °C.

dx.doi.org/10.1021/ma302220b | Macromolecules 2013, 46, 2725−2732

Table 1. Molecular Characteristics and Phase Transitions of P3AT-*b*-PMMA Block Copolymers

polymer[a]	N_{P3AT}[b]	N_{PMMA}[c]	PDI[d]	f_{PMMA}[e]	structure[f]	T_{OOT} (°C)	T_{ODT} (°C)	phase transition
$H_{21}M_{35}(0.49)$	21	35	1.11	0.49	LAM		210 ± 5	LAM → DIS
$D_{16}M_{47}(0.53)$	16	47	1.14	0.53	HEX	185 ± 5	215 ± 5	HEX → GYR → DIS
$E_{19}M_{47}(0.52)$	19	47	1.24	0.52	HEX	165 ± 5	180 ± 5	HEX → GYR → DIS
$E_{16}M_{35}(0.50)$	16	35	1.20	0.50	DIS			DIS

[a] $H_XM_Y(Z)$ is the designation of P3HT-*b*-PMMA with degree of polymerization (X unit) of P3HT, degree of polymerization (Y unit) of PMMA, and $f_{PMMA}(Z)$. While DM is the designation of P3DDT-*b*-PMMA, EM is the designation of P3EHT-*b*-PMMA. [b] As determined by ^{1}H NMR. [c] As determined by GPC analysis using PMMA standard. [d] As determined by GPC analysis using PS standard. [e] The volume fraction of PMMA (f_{PMMA}) of block copolymers was calculated from M_n of P3AT block and M_n of PMMA block. The density (ρ) of each polymer: ρ_{PMMA} = 1.19 g/mL,[55] ρ_{P3HT} = 1.11 g/mL,[56] ρ_{P3DDT} = 1.07 g/mL,[56] and ρ_{P3EHT} = 0.99 g/mL. [f] The structure (LAM = lamellae, HEX = hexagonally packed cylinders, GYR = gyroid, and DIS = disordered phase) was determined by SAXS at room temperature.

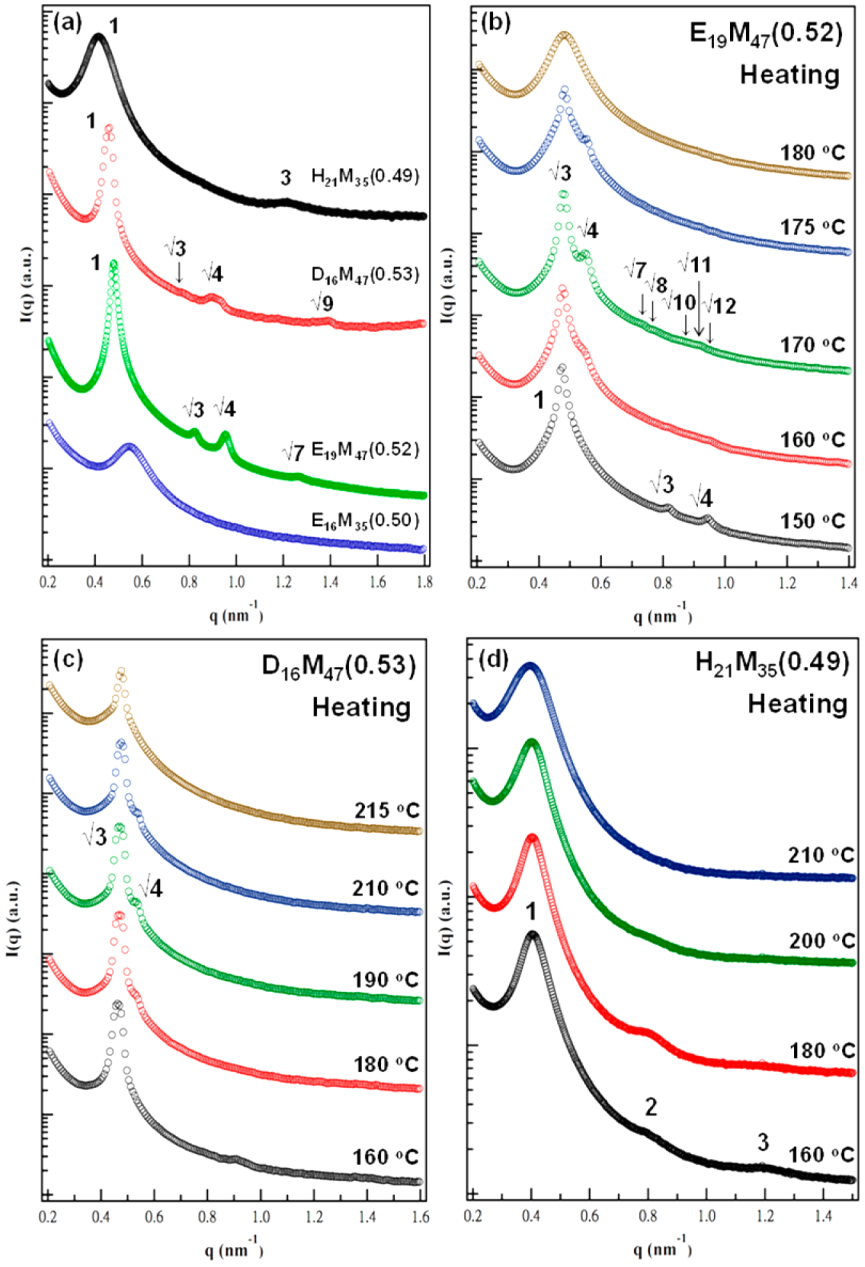

Figure 1. Versatile morphology of P3AT-*b*-PMMA at composition close to symmetry. (a) Synchrotron-SAXS profiles of P3AT-*b*-PMMA were measurd at 30 °C. After thermal annealing, the SAXS curves of block copolymers show various morphologies of these block copolyemrs near f_{PMMA} = 0.5. Phase transitions of copolymer were investigated using temperature-dependent SAXS measurements upon heating. (b) $E_{19}M_{47}(0.52)$, (c) $D_{16}M_{47}(0.53)$, and (d) $H_{21}M_{35}(0.49)$.

dx.doi.org/10.1021/ma302220b | *Macromolecules* 2013, 46, 2725−2732

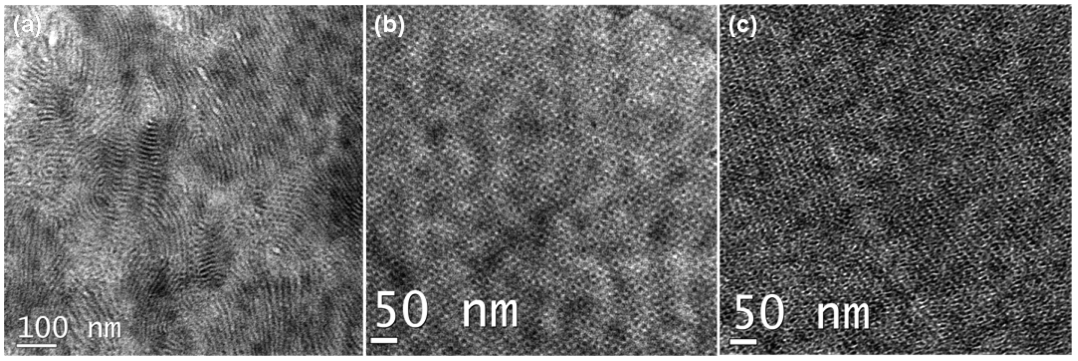

Figure 2. Morphology of P3DDT and P3EHT copolymers studied by TEM. (a) TEM micrograph of $D_{16}M_{47}(0.53)$ shows its morphology is hexagonal structure with different orientations of cylinders. TEM images of (b) $D_{16}M_{47}(0.53)$ and (c) $E_{19}M_{47}(0.52)$ were quenched from 190 and 170 °C, respectively, to preserve the gyroidal phase. Staining with RuO_4 reveals dark P3AT nanodomains and light PMMA nanodomains.

Figure 1c also shows the order−order transition of $D_{16}M_{47}(0.53)$ upon heating, from HEX to GYR. This gyroidal phase is further confirmed by TEM study (Figure 2b). Compared with our previous work of similar P3DDT-*b*-PMMA,[34] the formation of gyroidal phase shown here is less ordered. The result is due to the decreasing in segregation strength of $D_{16}M_{47}(0.53)$ with reduced degree of polymerization, and the sample is close to the disordered state. The copolymer with shorter side chain of hexyl rod segment exhibits totally different behavior. The morphology of $H_{21}M_{35}(0.49)$ upon heating shows lamellar phase without order−order transition before approaching the disordered state (Figure 1d).

It is interesting to note the appearance of nonlamellar phases of P3AT-*b*-PMMA at composition close to symmetry ($f_{PMMA} \approx 0.5$), which is not commonly observed in the rod−coil block copolymers. These results are similar to the self-assembly of coil−coil block copolymer such as POO-*b*-PEO[18] at high value of conformational asymmetry. For P3AT-*b*-PMMA, the conformational asymmetry is much associated with the spatial occupation of different alkyl side chain in P3AT block and clearly shifts the phase boundary. The influence of conformational asymmetry from P3AT block on the self-assembly behaviors can also explain the observation of hexagonal structures with high P3EHT fraction copolymers in P3EHT-*b*-PLA.[39] Although the conformational asymmetry has a strong effect on the phase behaviors of P3AT-*b*-PMMA, there are other factors such as competition between rod−rod and rod−coil interactions and crystallization-driven force which would be associated with final morphology. We will discuss these factors later.

The order−disorder transition temperature (T_{ODT}) of P3AT-*b*-PMMA block copolymer is determined by the disappearance of higher ordered Bragg reflective peaks in the temperature-dependent SAXS profiles (Figure 1) and by a discontinuous change in the intensity of the primary scattering peak in the vicinity of the order−disorder transition with temperature. In Figure 3, the divergences of SAXS scattering intensity of $H_{21}M_{35}(0.49)$, $D_{16}M_{47}(0.53)$, and $E_{19}M_{47}(0.52)$ are observed in the plot of inverse intensity vs inverse temperature, where the change of discontinuous will decide T_{ODT}. All the phase transition temperatures of P3AT-*b*-PMMA block copolymers are summarized in Table 1. Since T_{ODT} is associated with the segregation strength, the product of χN, for a block copolymer, we note that the transition temperature of P3EHT copolymer is lower than that of P3DDT and P3HT copolymers at similar N values, suggesting that the P3EHT segment has weaker

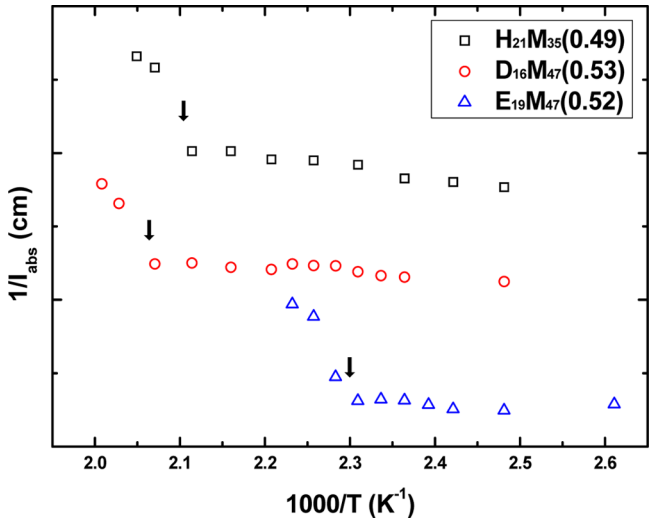

Figure 3. Inverse SAXS scattering intensity plotted as a function of inverse temperature for P3AT-*b*-PMMA. The discontinuity in the slope of curve indicats the order−disorder tansition (ODT), which is observed for $H_{21}M_{35}(0.49)$, $D_{16}M_{47}(0.53)$, and $E_{19}M_{47}(0.52)$.

repulsive interaction with PMMA segments as compared with P3HT and P3DDT. The result is contributed from different chemical structures of side chain in polythiophenes. We studied the value of fundamental parameters such as Flory−Huggins (rod−coil) interaction parameter (χ) and the competition between rod−rod and rod−coil interactions (G) of P3AT-*b*-PMMA model in order to correlate self-assembly behavior to the chemical structrue of rod−coil copolymer quantitatively.

Typically, the temperature dependence of Flory−Huggins interaction parameter can be described as

$$\chi = \chi_S + \chi_H/T \quad (1)$$

where χ_S is relative to entropic contribution and χ_H is an enthalpic term. With introducing alkyl side chain at the 3-position of thiophene ring, especially for the bulky 2-ethylhexyl side chain of P3EHT, it would lead to torsional defects or ring disorder along the polymer backbone, resulting in reduced chain stiffness of P3AT.[40] It has been proved by comparing Maire−Saupé μ parameters of P3ATs.[41] As a result, the chain conformations of P3ATs are semiflexible rods. On the basis of this, we adopted the random phase approximation (RPA) method to estimate the Flory−Huggins interaction parameter which has been used in polymer blends and classical coil−coil

dx.doi.org/10.1021/ma302220b | Macromolecules 2013, 46, 2725−2732

block copolymers extensively and also in rod−coil copolymers.[42] According to Leibler's Landau type mean-field theory modified for the effects of the molecular weight polydispersity and asymmetry in the segmental volume,[43−45] the observed scattering intensity in the disordered state is given by the equation

$$I_{obs}(q) = K[S(q)/W(q) - 2\chi N]^{-1} \quad (2)$$

where K is a constant and equations for $S(q)$ and $W(q)$ are described in the Supporting Information. By analyzing the structure factor of the SAXS curve measured in the disordered state, we can obtain the χ value from corresponding temperature above T_{ODT}. Since $E_{16}M_{35}(0.50)$ exhibits the disordered phase in the measured temperature window (from 110 to 150 °C), we could measure the empirical temperature dependence of χ between P3EHT and PMMA segments at relatively low temperatures (<150 °C). The fitting results are shown in Figure 4a. The linear regression of measured χ values (Figure 4b) can be obtained by the temperature-dependent equation of Flory−Huggins interaction parameter and gives the form $\chi = 0.0932 + 25.482/T$. We also employed the same method for both P3DDT-*b*-PMMA and P3HT-*b*-PMMA and measured the χ values from 240 to 250 °C for $D_{16}M_{47}(0.53)$ and from 223 to 230 °C for $H_{21}M_{35}(0.49)$, respectively. The fitting results and measured χ functions for $D_{16}M_{47}(0.53)$ and $H_{21}M_{35}(0.49)$ are $\chi = 0.0828 + 38.582/T$ and $\chi = 0.0433 + 56.370/T$, respectively, which are summarized in Table 2 and plotted in Figure 5.

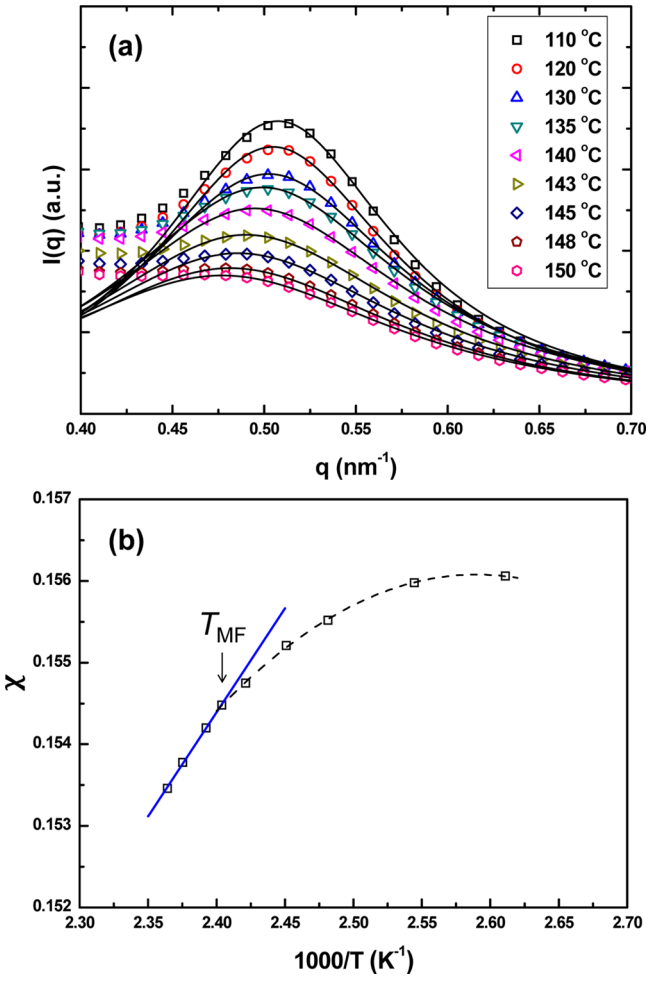

Figure 4. Estimation of empirical Flory−Huggins (rod−coil) interaction parameter of $E_{16}M_{35}(0.50)$ using random phase apprximation (RPA). (a) Temperature-dependent SAXS profiles (empty symbols) of $E_{16}M_{35}(0.50)$ are well fitted (solid lines), where only the primary peak in the disordered state is shown here. (b) Measured temperature dependence of χ is plotted with inverse temperature. The crossover point is denoted as mean-field theory temperature (T_{MF}), as indicated by arrow. The temperature points higher than T_{MF}, linear relationship part, are extracted, and χ is estimated as $\chi = 0.0932 + 25.482/T$.

Table 2. Comparison of Competition G Values in P3AT-*b*-PMMA

			G ($\equiv \mu/\chi$)		
polymer	μ_{P3AT}	$\chi_{P3AT/PMMA}$[a]	30 °C	130 °C	230 °C
$H_{21}M_{35}(0.49)$	$\mu_{P3HT} = -0.3 + 180/T$[a]	$\chi = 0.0433 + 56.370/T$	1.282	0.801	0.372
$D_{16}M_{47}(0.53)$	$\mu_{P3DDT} = -0.3 + 153/T$[b]	$\chi = 0.0828 + 38.582/T$	0.975	0.446	0.026
$E_{16}M_{35}(0.50)$	$\mu_{P3EHT} = -0.3 + 109/T$[b]	$\chi = 0.0932 + 25.482/T$	0.337		

[a]As measured in this work. [b]As obtained from ref 41.

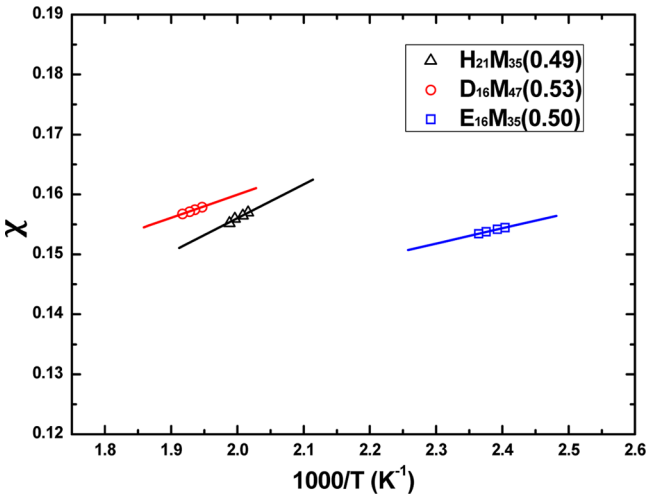

Figure 5. Temperature dependence of the Flory−Huggins interaction parameter between P3AT and PMMA segments for P3AT-*b*-PMMA. Extraction of a linear regression fitting measured χ values at different temperatures gives the empirical rod−coil interaction functional formulas, $\chi = 0.0433 + 56.370/T$ for $H_{21}M_{35}(0.49)$ (black line), $\chi = 0.0828 + 38.582/T$ for $D_{16}M_{47}(0.53)$ (red line), and $\chi = 0.0932 + 25.482/T$ for $E_{16}M_{35}(0.50)$ (blue line).

A complicated phase diagram of rod−coil block copolymer has been observed due to the competition between the rod−rod interaction and the rod−coil interaction, resulting in the shift of phase boundary.[46−48] For rodlike polymer DEH−PPV, the Maier−Saupé (rod−rod) interaction parameter (μ) is measured by extraction of a linear regression fitting to the observed nematic−isotropic transition temperatures at different molecular weight with an assumption of pure rod conformation.[49] The rod−rod interaction parameters of P3DDT and P3EHT have been estimated by the same method in the literature, and P3EHT has reduced interaction strength ca. 33% lower than P3DDT due to its branch alkyl chain.[41] The strength of rod−rod interaction of P3HT with high molecular weight cannot be defined since its nematic−isotropic transition

dx.doi.org/10.1021/ma302220b | Macromolecules 2013, 46, 2725−2732

temperature is too high to be actually determined which is approaching its thermal decomposition temperature. In order to compare the G values of three kinds of P3AT-*b*-PMMA block copolymers affected by the different chemical structures in P3AT segments, we determined the Maier−Saupé interaction parameter of P3HT with relatively low molecular weight (≤18 units) via the same process and obtained the equation $\mu_{P3HT} = -0.3 + 180/T$ (see Table S1 and Figure S2 of Supporting Information).

The G value represents the competition between rod−rod and rod−coil interactions ($G \equiv \mu/\chi$) of the rod−coil block copolymer, which is one of the important determining factors for self-assembly behaviors of block copolymers. Since both Flory−Huggins and Maier−Saupé interaction parameters are temperature-dependent, the G values of P3AT-*b*-PMMA would be changed with temperatures. However, the Maier−Saupé interaction value of P3EHT becomes negative above 90 °C,[41] resulting in the negative G value of P3EHT-*b*-PMMA. Thus, we compared their relative interaction strengths at 30 °C. The results are summarized in Table 2. The P3EHT-*b*-PMMA has the lowest G value among these three block copolymers with the value of 0.337, indicating that the rod−rod interaction between P3EHT rods is much smaller than the rod−coil interaction between P3EHT and PMMA segments. It suggests the morphology of P3EHT-*b*-PMMA might be dominated by microphase separation. In contrast, P3HT-*b*-PMMA has the largest G parameter with the value of 1.282, resulting from slightly stronger rod−rod interaction of P3HT compared to P3HT/PMMA interaction. If the rod−rod interaction is much larger than the rod−coil interaction, the phase behavior of copolymer will show lamellar structure and liquid crystalline structure in a large range of coil fractions such as weakly segregated DEH-PPV-*b*-PI rod−coil block copolymer. The μ value of DEH-PPV segments is roughly 50 times larger than the χ value between DEH−PPV and PI.[42]

However, the comparison of relative G values for P3AT-*b*-PMMA at 30 °C may be somewhat irrelevant because both P3AT and PMMA blocks are not in the melt. In terms of this, we determined the G values of P3DDT-*b*-PMMA and P3HT-*b*-PMMA at 130 and 230 °C, respectively. They have shown a similar trend as at 30 °C. For P3DDT-*b*-PMMA, it has the G value of 0.446 at 130 °C, suggesting microphase separation would dominate the morphology. When $D_{16}M_{47}(0.53)$ cooled from the melt, the glassy PMMA blocks would form prior to crystallizaion of P3DDT blocks, which might result in poor crystalline structure of P3DDT within hexagonal nanodomains. For P3HT-*b*-PMMA at 230 °C, the P3HT/PMMA interaction is also stronger than the interaction between P3HT rods. But unlike $D_{16}M_{47}(0.53)$, the P3HT segment in $H_{21}M_{35}(0.49)$ would undergo crystallization before vitrification of PMMA segment during cooling process due to its strong crystallization-driven froce. It would break down the morphology into lamellar or fibril structures, which might be associated with ususal morphology observed within P3HT-containing block copolymers.[50,51]

Although we have quantitatively determined the rod−coil interactions of P3AT-*b*-PMMA block copolymers by using the random phase approximation method, some issues still worth noting. Using the classical random phase approximation model which is based on the block copolymer with Gaussian coils may be sufficient in this research to estimate the χ value between semiflexible P3AT and coil PMMA. Additionally, from the theoretical prediction,[47] it indicates that the effect of small value of μ on the spinodal value of Flory−Huggins χ parameter can be ignored. The values of the Maier−Saupé μ parameter for P3DDT and P3EHT are negative in the measured temperature window, indicating these two μ values are extremely small that we can ignore the influence of their rod−rod interactions on the estimation of χ values for P3DDT-*b*-PMMA and P3EHT-*b*-PMMA. As a consequence, it might be reasonable for us to conduct RPA model to estimate χ value for P3AT-*b*-PMMA in the disordered phase, though the μ value of P3HT may not be small enough to be ignored in the measured temperature window. Therefore, there is still uncertainty to estimate G values of P3AT-*b*-PMMA block copolymers, but it shows the trend for the effect of side chain structures of polythiophenes on the morphology via simultaneously tuning rod−rod and rod−coil interactions.

The crystallization-dominated phase behavior is commonly observed in conventional crystalline−amorphous block copolymers.[52−54] In our previous work of P3DDT-*b*-PMMA,[34] the melting point of P3DDT block was shifted to lower temperature with reduced crystallinity due to the confinement of P3DDT segments within cylindrical nanodomains. As temperature increased, the P3DDT crystalline segments first melted in the cylinders, and then morphology transformed into gyroid above the glass transition temperature (T_g) of PMMA segments. A similar correlation between crystallinity and transition temperature is observed for both $E_{19}M_{47}(0.52)$ and $D_{16}M_{47}(0.53)$. Figure 6a shows the melting points of $D_{16}M_{47}(0.53)$ and $E_{19}M_{47}(0.52)$ are absent in the DSC thermograms, indicating that the crystallinity of either P3DDT or P3EHT is poor. The results are consistent with their wide-angle X-ray scattering (WAXS) profiles as shown in the Figure 6b, where only the (100) reflection for P3DDT block is clearly observed. It suggests that slight crystalline structure of P3DDT segment is present within the constrained cylinders of $D_{16}M_{47}(0.53)$. The crystallization of polythiophene block has resist forces imposed from the PMMA extremely glassy domains. The similar results are also found in the P3HT-*b*-P2VP system, where the order−order transition occurs at a 68% P2VP volume fraction with poor crystallization of polythiophene segments.[37] However, for $H_{21}M_{35}(0.49)$, both results of DSC and WAXS display the P3HT segments are well crystallized within the lamellar structure. In addition, the DSC curve of P3HT-*b*-PMMA shows a glass transition of P3HT block at around 150 °C, which is similar to the corresponding homo-P3HT (Figure S3). Altogether, the tunable crystallization-driven force arising from P3AT segments has a strong influence on the morphologies for P3AT-*b*-PMMA block copolymers.

■ CONCLUSIONS

In summary, we have demonstrated that by altering the chemical structures of rod−coil block copolymers, one can simultaneously adjust the rod−rod interaction, rod−coil interaction, and conformational asymmetry to obtain various self-assembly nanostructures. The block copolymers of P3AT-*b*-PMMA were used as model molecules. Under the rational molecular design, the versatile self-assembly morphology of P3AT-*b*-PMMA is observed at composition near symmetry, including lamellar and hexagonal structures, cylinder-to-gyroid phase transition, and disordered state. The presence of nonlamellar phase around $f_{P3AT} = 0.5$ is associated with the conformational asymmetry between P3AT and PMMA segments, which is contributed from the spatial occupation of

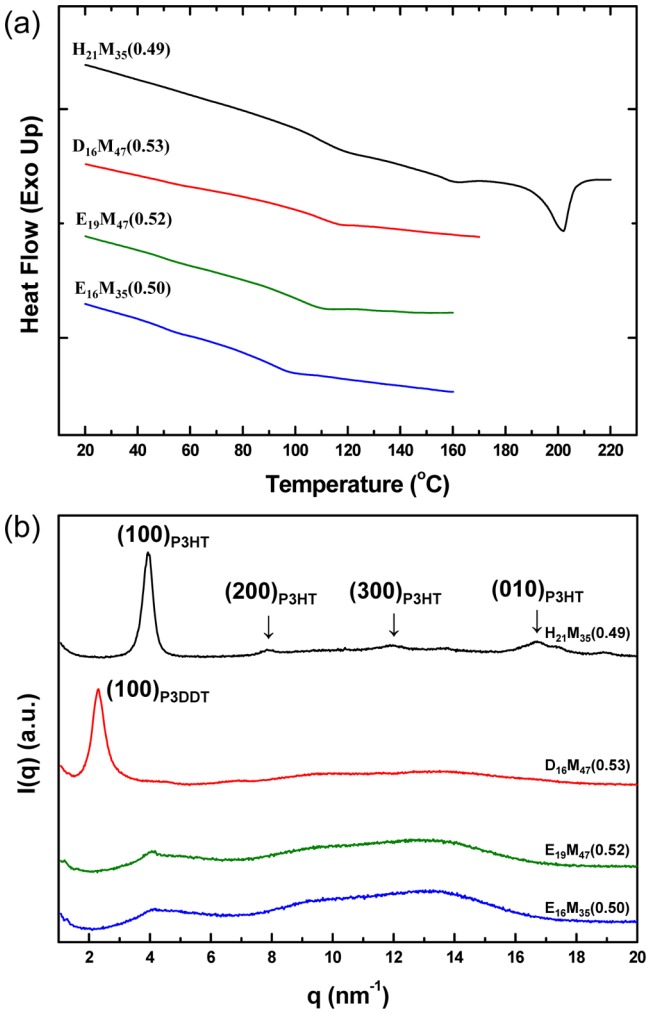

Figure 6. Study of crystallization of P3AT-*b*-PMMA block copolymers. (a) DSC thermograms of P3AT-*b*-PMMA block copolymers with a scan heating rate of 10 °C/min. While $H_{21}M_{35}(0.49)$ exhibits a significant monoendothermic peak at 200 °C, indicating a melting point without liquid crystalline transition, only the glass transition temperature at around 100 °C is observed for other three block copolymers. (b) WAXS profiles of P3AT-*b*-PMMA block copolymers were measured at room temperature. The $H_{21}M_{35}(0.49)$ shows the well crystalline structure with (*h*00) and (010) reflections.

different alkyl side chain of P3ATs and is accompanied by reduced *G* value and reduced crystallization-driven force. The knowledge obtained here can provide new insights into the self-assembly behaviors of rod−coil block copolymer qualitatively and quantitatively to rational design and manipulate the desired order structures for further advances in organic optoelectronics, biosensors, and other applications.

EXPERIMENTAL SECTION

Materials. A series of the poly(3-alkylthiophene)-*b*-poly(methyl methacrylate) (P3AT-*b*-PMMA) rod−coil diblock copolymers (Scheme 1) with nearly compositional symmetry were synthesized via click reaction in three steps according to the similar synthetic routes in previous literatures.[34−36] In brief, we took P3DDT-*b*-PMMA as an example. The azido-ended PMMA was first synthesized by using anionic polymerization and terminated with coupling agent α,α'-dibromo-*p*-xylene, followed by reacting with sodium azide. Second, the alkyne-terminated P3DDT was prepared using GRIM, followed by adding ethynylmagnesium bromide to terminate living P3DDT chain. Finally, high reactivity and high yield "click" chemistry was used to connect both azido-terminated PMMA and excess alkyne-terminated P3DDT blocks. Thus, purified block copolymer was obtained after precipitation three times in hexane and flash chromatography with neutral alumina oxide, followed by characterization by GPC and ^{1}H NMR (see Figure S4). The molecular weight, polydispersity index, and volume fraction for all P3AT-*b*-PMMA polymers are listed in Table 1. Self-assembly of all samples were studied after thermal annealing. While P3DDT-*b*-PMMA and P3EHT-*b*-PMMA copolymers were annealed at 140 °C for 2 days, P3HT-*b*-PMMA was annealed at 210 °C for 10 min and then at 180 °C for 2 days.

Density. The density of P3EHT was determined around 0.99 g/mL using a Mettler Toledo XP/XS balance equipped with a density measurement kit. For other polymers, the density values were used from the literatures: PMMA (1.19 g/mL),[55] P3HT (1.11 g/mL),[56] and P3DDT (1.07 g/mL).[56]

DSC. For the differential scanning calorimetry (DSC) experiment, a TA Instruments Q200 was used to probe thermal transition of P3AT-*b*-PMMA block copolymers. Self-assembled samples after annealing were prepared into a DSC pan with ca. 5 mg. During DSC analysis samples were heated at a rate of 10 °C/min.

SAXS/WAXS. The morphologies and thermal induced phase transitions were probed by the temperature-dependent SAXS experiments performed at the beamline BL23A1 of the National Synchrotron Radiation Research Center (NSRRC), Taiwan. The energy of X-ray source was 8 keV. The scattering signals were collected by a MarCCD detector of both 512 × 512 and 1024 × 1024 pixel resolution. The scattering intensity profile was output as the plot of the scattering intensity I versus the scattering vector q ($q = (4\pi/\lambda)\sin(\theta)$). Samples were placed into a 1 mm thick washer between two Kapton sheets and thermally annealed under a nitrogen atmosphere. The SAXS profiles were corrected for the incident beam intensity and the background from the thermal diffuse scattering. For temperature-dependent experiments, the samples were held for at least 10 min at each temperatures followed by data acquisition. The Flory−Huggins interaction parameters for all block copolymers were estimated by fitting the structure factor of observed SAXS scattering curves (I_{obs}) in the disordered state, which are described in detail in the Supporting Information. The crystalline structures of P3AT blocks in P3AT-*b*-PMMA were studied by WAXS measurements at the beamline BL13A of NSRRC.

TEM. Samples for TEM were first thermally annealed with the same conditions described in the SAXS experiment and then quenched from the temperature of formation of gyroidal phase for P3DDT-*b*-PMMA and P3EHT-*b*-PMMA copolymers. The quenched samples were microtomed to form 60−70 nm slices and stained by exposure to the vapor of RuO_4 solution for 5 min. Because of preference for staining within P3AT nanodomains, the enhanced contrast of image was obtained. TEM images were taken with a JEOL 1400 microscope operated at an accelerating voltage of 100 kV.

ASSOCIATED CONTENT

Supporting Information

Detailed description of SAXS data analysis for measuring Flory−Huggins (rod−coil) interaction parameter, characterization of block copolymers, and estimation of Maier−Saupé (rod−rod) interaction parameter of P3HT. This material is available free of charge via the Internet at http://pubs.acs.org.

AUTHOR INFORMATION

Corresponding Author

*E-mail: ccho76@ntu.edu.tw (C.C.H.); suwf@ntu.edu.tw (W.F.S.).

Notes

The authors declare no competing financial interest.

■ ACKNOWLEDGMENTS

We gratefully thank the financial support from the National Science Council of Taiwan (99-2221-E-002-020-MY3 and 101-2120-M-002-003). We also acknowledge the Department of Chemistry and College of Bioresources and Agriculture of National Taiwan University for the use of its NMR spectrometer and TEM microscope, respectively. We sincerely thank Dr. U-Ser Jeng, Dr. Chun-Jen Su, and Dr. Ming-Tao Lee for help with the SAXS and WAXS experiments at NSRRC.

■ REFERENCES

(1) Bates, F. S.; Hillmyer, M. A.; Lodge, T. P.; Bates, C. M.; Delaney, K. T.; Fredrickson, G. H. *Science* **2012**, *336*, 434−440.
(2) Tang, C.; Lennon, E. M.; Fredrickson, G. H.; Kramer, E. J.; Hawker, C. J. *Science* **2008**, *322*, 429−432.
(3) Li, L.; Shen, X.; Hong, S. W.; Hayward, R. C.; Russell, T. P. *Angew. Chem., Int. Ed.* **2012**, *51*, 4089−4094.
(4) Majewski, P. W.; Gopinadhan, M.; Jang, W. S.; Lutkenhaus, J. L.; Osuji, C. O. *J. Am. Chem. Soc.* **2010**, *132*, 17516−17522.
(5) Botiz, I.; Darling, S. B. *Mater. Today* **2010**, *13*, 42−51.
(6) Segalman, R. A.; McCulloch, B.; Kirmayer, S.; Urban, J. J. *Macromolecules* **2009**, *42*, 9205−9216.
(7) Zhao, Y.; Thorkelsson, K.; Mastroianni, A. J.; Schilling, T.; Luther, J. M.; Rancatore, B. J.; Matsunaga, K.; Jinnai, H.; Wu, Y.; Poulsen, D.; Fréchet, J. M. J.; Alivisatos, A. P.; Xu, T. *Nat. Mater.* **2009**, *8*, 979−985.
(8) Sommer, M.; Lindner, S. M.; Thelakkat, M. *Adv. Funct. Mater.* **2007**, *17*, 1493−1500.
(9) Crossland, E. J. W.; Kamperman, M.; Nedelcu, M.; Ducati, C.; Wiesner, U.; Smilgies, D. M.; Toombes, G. E. S.; Hillmyer, M. A.; Ludwigs, S.; Steiner, U.; Snaith, H. J. *Nano Lett.* **2009**, *9*, 2807−2812.
(10) Darling, S. B. *Energy Environ. Sci.* **2009**, *2*, 1266−1273.
(11) Yen, W. C.; Lee, Y. H.; Lin, J. F.; Dai, C. A.; Jeng, U. S.; Su, W. F. *Langmuir* **2011**, *27*, 109−115.
(12) Meuler, A. J.; Hillmyer, M. A.; Bates, F. S. *Macromolecules* **2009**, *42*, 7221−7250.
(13) Khandpur, A. K.; Förster, S.; Bates, F. S.; Hamley, I. W.; Ryan, A. J.; Brass, W.; Almdal, K.; Mortensen, K. *Macromolecules* **1995**, *28*, 8796−8806.
(14) Vavasour, J. D.; Whitmore, M. D. *Macromolecules* **1993**, *26*, 7070−7075.
(15) Matsen, M. W.; Schick, M. *Macromolecules* **1994**, *27*, 4014−4015.
(16) Bates, F. S.; Schulz, M. F.; Khandpur, A. K.; Förster, S.; Rosedale, J. H.; Almdal, K.; Mortensen, K. *Faraday Discuss. Chem. Soc.* **1994**, *98*, 7−18.
(17) Matsen, M. W.; Bates, F. S. *J. Polym. Sci., Part B: Polym. Phys.* **1997**, *35*, 945−952.
(18) Hamley, I. W.; O'Driscoll, B. M. D.; Lotze, G.; Moulton, C.; Allgaier, J.; Frielinghaus, H. *Macromol. Rapid Commun.* **2009**, *30*, 2141−2146.
(19) Liu, J.; Haynes, D.; Balliet, C.; Zhang, R.; Kowalewski, T.; McCullough, R. D. *Adv. Funct. Mater.* **2012**, *22*, 1024−1032.
(20) Lin, S. T.; Tung, Y. C.; Chen, W. C. *J. Mater. Chem.* **2008**, *18*, 3985−3992.
(21) Olsen, B. D.; Segalman, R. A. *Macromolecules* **2005**, *38*, 10127−10137.
(22) Houbenov, N.; Haataja, J. S.; Iatrou, H.; Hadjichristidis, N.; Ruokolainen, J.; Faul, C. F. J.; Ikkala, O. *Angew. Chem., Int. Ed.* **2011**, *50*, 2516−2520.
(23) Minich, E. A.; Nowak, A. P.; Deming, T. J.; Pochan, D. J. *Polymer* **2004**, *45*, 1951−1957.
(24) Chen, J. T.; Thomas, E. L.; Ober, C. K.; Mao, G. P. *Science* **1996**, *273*, 343−346.
(25) Lee, M.; Cho, B. K.; Zin, W. C. *Chem. Rev.* **2001**, *101*, 3869−3892.
(26) Sary, N.; Mezzenga, R.; Brochon, C.; Hadziioannou, G.; Ruokolainen, J. *Macromolecules* **2007**, *40*, 3277−3286.
(27) Olsen, B. D.; Segalman, R. A. *Mater. Sci. Eng., R* **2008**, *62*, 37−66.
(28) Chen, X. F.; Shen, Z. H.; Wan, X. H.; Fan, X. H.; Chen, E. Q.; Ma, Y. G.; Zhou, Q. F. *Chem. Soc. Rev.* **2010**, *39*, 3072−3101.
(29) Sary, N.; Rubatat, L.; Brochon, C.; Hadziioannou, G.; Ruokolainen, J.; Mezzenga, R. *Macromolecules* **2007**, *40*, 6990−6997.
(30) Sary, N.; Brochon, C.; Hadziioannou, G.; Mezzenga, R. *Eur. Phys. J. E* **2007**, *24*, 379−384.
(31) Ho, C. C.; Lee, Y. H.; Dai, C. A.; Segalman, R. A.; Su, W. F. *Macromolecules* **2009**, *42*, 4208−4219.
(32) Chang, C. J.; Lee, Y. H.; Chen, H. L.; Chiang, C. H.; Hsu, H. F.; Ho, C. C.; Su, W. F.; Dai, C. A. *Soft Matter* **2011**, *7*, 10951−10960.
(33) Olsen, B. D.; Segalman, R. A. *Macromolecules* **2007**, *40*, 6922−6929.
(34) Lin, S. H.; Ho, C. C.; Su, W. F. *Soft Matter* **2012**, *8*, 4890−4893.
(35) Jeffries-El, M.; Sauve, G.; McCullough, R. D. *Adv. Mater.* **2004**, *16*, 1017−1019.
(36) Ho, C. C.; Dai, C. A.; Su, W. F. *J. Appl. Polym. Sci.* **2009**, *111*, 1571−1580.
(37) Lee, Y. H.; Yen, W. C.; Su, W. F.; Dai, C. A. *Soft Matter* **2011**, *7*, 10429−10442.
(38) Dai, C. A.; Yen, W. C.; Lee, Y. H.; Ho, C. C.; Su, W. F. *J. Am. Chem. Soc.* **2007**, *129*, 11036−11038.
(39) Ho, V.; Boudouris, B. W.; McCulloch, B. L.; Shuttle, C. G.; Burkhardt, M.; Chabinyc, M. L.; Segalman, R. A. *J. Am. Chem. Soc.* **2011**, *133*, 9270−9273.
(40) Darling, S. B. *J. Phys. Chem. B* **2008**, *112*, 8891−8895.
(41) Ho, V.; Boudouris, B. W.; Segalman, R. A. *Macromolecules* **2010**, *43*, 7895−7899.
(42) Olsen, B. D.; Shah, M.; Ganesan, V.; Segalman, R. A. *Macromolecules* **2008**, *41*, 6809−6817.
(43) Leibler, L. *Macromolecules* **1980**, *13*, 1602−1617.
(44) Sakurai, S.; Mori, K.; Okawara, A.; Kimishims, K.; Hashimoto, T. *Macromolecules* **1992**, *25*, 2679−2691.
(45) Feldman, K. E.; Kade, M. J.; Meijer, E. W.; Hawker, C. J.; Kramer, E. J. *Macromolecules* **2010**, *43*, 5121−5127.
(46) Reenders, M.; ten Brinke, G. *Macromolecules* **2002**, *35*, 3266−3280.
(47) Singh, C.; Goulian, M.; Liu, A. J.; Fredrickson, G. H. *Macromolecules* **1994**, *27*, 2974−2986.
(48) Holyst, R.; Schick, M. *J. Chem. Phys.* **1992**, *96*, 730−740.
(49) Olsen, B. D.; Jang, S. Y.; Lüning, J. M.; Segalman, R. A. *Macromolecules* **2006**, *39*, 4469−4479.
(50) Moon, H. C.; Anthonysamy, A.; Lee, Y.; Kim, J. K. *Macromolecules* **2011**, *44*, 1894−1899.
(51) Botiz, I.; Darling, S. B. *Macromolecules* **2009**, *42*, 8211−8217.
(52) Lin, M. C.; Nandan, B.; Chen, H. L. *Soft Matter* **2012**, *8*, 3306−3322.
(53) Ho, R. M.; Chiang, Y. W.; Chen, C. K.; Wang, H. W.; Hasegawa, H.; Akasaka, S.; Thomas, E. L.; Burger, C.; Hsiao, B. S. *J. Am. Chem. Soc.* **2009**, *131*, 18533−18542.
(54) Loo, Y. L.; Register, R. A.; Ryan, A. J. *Macromolecules* **2002**, *35*, 2365−2374.
(55) Shetter, J. A. *J. Polym. Sci., Part B: Polym. Lett.* **1963**, *1*, 209−213.
(56) Tashiro, K.; Ono, K.; Minagawa, Y.; Kobayashi, M.; Kawai, T.; Yoshino, K. *J. Polym. Sci., Part B: Polym. Phys.* **1991**, *29*, 1223−1233.